Available online at www.sciencedirect.com
ScienceDirect
International Journal of Machine Tools & Manufacture 48 (2008) 485–498
INTERNATIONAL JOURNAL OF MACHINE TOOLS & MANUFACTURE DESIGN, RESEARCH AND APPLICATION
www.elsevier.com/locate/ijmactool

Numerical modeling of advanced materials

T. Meinders[a,*], E.S. Perdahcıoğlu[a,b,c], M. van Riel[a,b], H.H. Wisselink[a,b]

[a]University of Twente, P.O. Box 217, 7500AE Enschede, The Netherlands
[b]Netherlands Institute for Metals Research, P.O. Box 5008, 2600GA Delft, The Netherlands
[c]Foundation for Fundamental Research on Matter, P.O. Box 3021, 3502GA Utrecht, The Netherlands

Received 23 February 2007; accepted 10 August 2007
Available online 19 August 2007

Abstract

The finite element (FE) method is widely used to numerically simulate forming processes. The accuracy of an FE analysis strongly depends on the extent to which a material model can represent the real material behavior. The use of new materials requires complex material models which are able to describe complex material behavior like strain path sensitivity and phase transformations. Different yield loci and hardening laws are presented in this article, together with experimental results showing this complex behavior. Recommendations on how to further improve the constitutive models are given. In the area of damage and fracture behavior, a non-local damage model is presented, which provides a better prediction of sheet failure than the conventional Forming Limit Diagram.

Keywords: Strain path dependency; Phase transformations; Non-local damage models; FLC; Sheet metal forming

1. Introduction

During the few last decades, the sheet metal forming industry tends to favor light construction principles, leading to the usage of new materials like aluminum, sandwich laminates, High Strength Steel and metastable steels. Without extensive knowledge of the materials used, it is hardly possible to adequately design the forming tools and make a proper choice of blank material to manufacture a product with the desired shape and performance. As a result, a costly and time consuming trial- and error-process is started to determine the proper process design leading to the desired product. To accelerate the product time to market, process modeling by computer simulation can be used to replace the experimental trial- and error-process by a virtual trial- and error-process. Rapid developments in computer hardware make the finite element (FE) analysis of complex deformation responses increasingly applicable. Although FE Programs are quite sophisticated nowadays, their accuracy and reliability do not yet satisfy the industrial requirements. The main reasons are the lack of knowledge of the behavior of the applied new materials and the inaccuracy of the used numerical algorithms (e.g. numerical integration, element formulation). As a result, the FE method is not sufficiently capable of simulating forming processes. Therefore, research is necessary to improve the usability of numerical simulations in sheet metal forming.

This article focuses on some recent developments in the field of material characterization. To improve the constitutive modeling of metals, more flexible and more material-specific yield loci and hardening laws compared to the conventional models are needed. Section 2 describes the current state of progress in this field. Both an experimental setup and material models, which account for complex material behavior like strain path dependency and phase transformations, are presented. Another field of interest is the damage and fracture behavior of material during sheet forming. A commonly used method to predict geometrical instabilities is the forming limit curve (FLC). However, the use of an FLC has some limitations. To improve the prediction of failure, ductile damage models can be used instead or complementary to the FLC approach, as

*Corresponding author.
E-mail address: v.t.meinders@ctw.utwente.nl (T. Meinders).

0890-6955/$ - see front matter © 2007 Elsevier Ltd. All rights reserved.
doi:10.1016/j.ijmachtools.2007.08.005

mentioned in Section 3. The article finishes with some concluding remarks and future trends.

2. Material characterization

Section 2.1 begins with a theoretical introduction of the stress–strain behavior of stable and metastable materials. Section 2.2 shows how this stress–strain behavior can be captured in numerical models to be able to describe the material behavior as accurately as possible. Material data is required as input data for these material models. The more complex the material models become, the more complex is the material data required. Some recipes to obtain this data are treated in Section 2.3.

2.1. Material physics

2.1.1. Yield loci

A yield surface encloses the elastic region in a multi-axial stress space. The yield surface also predicts anisotropic behavior of the material, also indicating that the yield surface should be chosen according to the material behavior. Yield criteria are developed from the onset of material modeling. A still widely used model is the Tresca model which shows good correspondence to the behavior of aluminum. The Hill'48 model is more suited to steels and is more flexible than the Tresca model. Besides modeling the elasto-plastic transition of the material, yield loci are used to determine FLCs for failure, see Section 3.1.

Currently, two groups of yield surfaces can be distinguished. The first group contains yield descriptions that are specifically developed for certain materials and are determined by the yield stress in the uniaxial tensile test and 1 or 2 additional parameters [1,2]. The other group consists of yield surfaces that are flexible, and hence are able to describe multiple materials, but require more input [3,4]. The Vegter yield-criterion (a member of the latter group) is developed for sheet material characterization and is a typical macro-scale description of the yield surface.

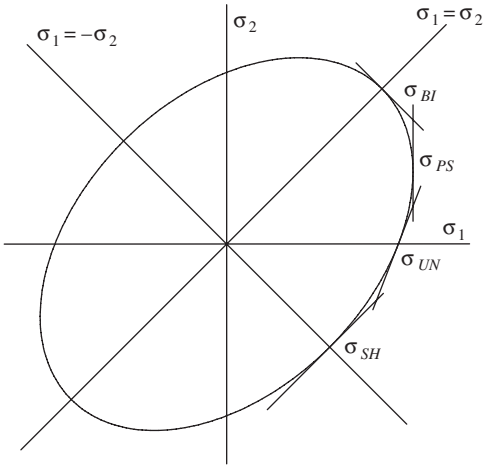

Fig. 1. The Vegter yield surface with the four test points.

As illustrated in Fig. 1 the yield criterion combines the results of four tests; simple shear test, tensile test, plane strain test and the biaxial test. Bezier interpolation between these four reference points is used to describe the yield surface. Assuming that the material exhibits the same behavior in compression as in tension, makes the yield surface symmetrical around the line $\sigma_1 = -\sigma_2$ (principal stresses). Furthermore, the region where $\sigma_1 > \sigma_2$ is the same as the region where $\sigma_2 > \sigma_1$, but with the specimen rotated 90°. So the yield surface is symmetric around the lines $\sigma_1 = -\sigma_2$ and $\sigma_1 = \sigma_2$. Planar anisotropic behavior is modeled by making all reference points dependent on the rolling direction. Consequently, tests have to be performed in different directions.

A challenge in developing new yield criteria is to minimize the number of parameters, and hence the number of required tests, while having a satisfactory flexibility in the criterion.

2.1.2. Work hardening

The yield surface, as described in the previous section, is however not a static boundary. The yield surface changes due to plastic deformation. Changes one can think of are enlargement, shape change, rotation or translation in stress space of the yield surface and all kinds of combinations. The underlying mechanism of yield surface changes can be found in the microstructure of the material. During plastic deformation, microstructural developments and—with increasing strain—also texture lead to work hardening of the material. The strength of the material increases which makes this phenomenon useful. However, with increasing strain, the amount of plastic strain can become too high and the material will fail.

The microstructural developments are initiated with the formation of a small cellular structure. Enforced by the deformation, dislocations migrate through the material and form boundaries of dislocations that envelop volumes having relatively small concentrations of dislocations. This process starts already at strains of 1% or 2%. With increasing strain, dislocation sheets [5] are developed approximately parallel to the most active slip systems. They consist of dislocations that are fixed in the plane and contribute to further hampering of the deformation. Because the dislocation sheets have a specific direction with respect to the deformation direction, they contribute to the strain path sensitivity of the material. With increasing strain more dislocations migrate towards the dislocation sheets and get stuck there. Microbands [6–8] develop and create opportunities for dislocations to migrate through the dislocation sheets. With increasing strain the microbands evolve into dislocation sheets.

As a metal undergoes more severe deformation, a preferred direction or texture develops [9]. Certain crystallographic planes are oriented in a preferred manner with respect to the direction of maximum strain. The type of texture that develops depends primarily on the number and type of slip planes. Depending on the type of texture the

anisotropy factor can increase and thereby enhance deep drawability [10].

2.1.3. Metastable steels

'Metastable' is a thermodynamics term used to describe a phase that is not the most stable one at the current temperature and pressure conditions and additionally does not have sufficient free energy to transform into the most stable one. Metastable steels earn their name because of the metastable austenite phase they comprise. Austenite can be retained at room temperature partially or completely after the annealing process with the help of chemical constituents such as chromium and nickel. These constituents are found in austenitic stainless steels and make that type of steels metastable in the sense that the austenite can transform into martensite if sufficient free energy is supplied. Steels like AISI 304, 316 and ASTM-A 564 are called TRIP (TRansformation Induced Plasticity) steels because under plastic deformation the retained austenite transforms into martensite, during which additional plastic deformation is gained.

In addition to the plasticity gained by transformation, the yield strength of the steel increases significantly due to the increasing amount of martensite, resulting in an unusual stress–strain behavior as shown in Fig. 2. In the figure it can be observed that it is possible to achieve very high strength levels with little loss of formability with these materials. Besides, due to their chemical composition they are highly corrosion resistant. These properties make them very favorable for industrial applications. However, it can also be deduced from Fig. 2 that it is hard to fit conventional material models which use a simple yield surface and a hardening law to model their behavior.

Before transformation, ideally, the material consists of equally sized and shaped austenite grains. Upon transformation, within these grains, martensite plates, needles or laths (further on all these shapes will be referred to as plates) start forming. The transformation itself is very rapid and approaches the speed of sound in solids. These plates grow instantly until they reach an obstacle such as a grain boundary or another plate. Thus, the material after transformation comprises of plates of martensite bounded by imaginary grains and these plates are of various sizes since the space available for new ones decreases with proceeding transformation [12].

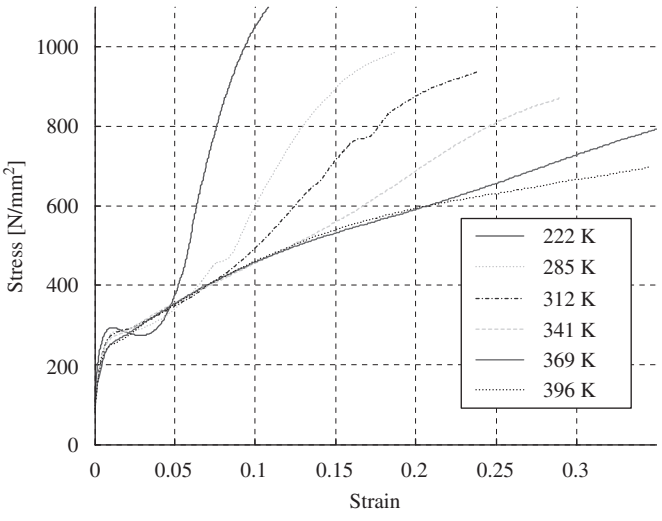

Fig. 2. Stress–strain curves of ASTM-A 564 TRIP steel at different temperatures [11].

The reason austenite is trapped in the matrix and cannot transform into martensite is the elastic strain necessary to deform the matrix during transformation. Martensite is lower in density, so there must be enough free energy to cover for the bulk straining of the surrounding when a martensitic plate forms. Additionally, the lattice rearrangement from austenite to martensite requires shear deformation. The matrix therefore is strained in shear which requires additional free energy. The required mechanical energy (mechanical driving force) can be calculated at different temperatures [13].

In addition to lattice straining and the calculation of the mechanical driving force, one very important point to consider is the fact that martensite nucleates heterogeneously in the matrix. That is, it is not possible for martensite plates to form anywhere in the bulk, but some heterogeneity is required in the form of lattice distortions. This phenomenon is proven experimentally and there are widely accepted formulations that govern the nucleation theory of martensite [14,15]. This fact has also been regarded considering the strain-induced transformations by Olson and Cohen who considered the shear-band intersections as the main nucleation sites for martensite and formulated the progression of the transformation based on the number and availability of these sites [16].

There exist a number of algorithms for simulation of this phenomenon. Some are empirical in their nature and rely on experimental results to fit the results [11]. However, once fit they produce very reliable outputs as far as the material remains the same. These models are very sensitive to material properties and a small change in a property can cause significant errors in the analysis. On the other hand, there are models that take the above mentioned phenomena into account and are scientifically more explanatory. They rely on some of the phenomena introduced above but because of the complexity of integration it is usually not possible to consider all of them at once.

2.2. Material modeling

2.2.1. Yield loci and hardening laws

In numerical computations, a yield function ϕ is commonly used. The equation $\phi = 0$ represents the situation where the stress state is on the yield surface; in this situation plastic deformation is possible. If $\phi < 0$ the material is in the elastic region, whereas $\phi > 0$ is infeasible. The yield stress σ_y (a measure for the size of the yield surface) describes the isotropic hardening of the material and can be determined by the stress–strain curve of a

uniaxial tensile test. Also a corresponding hardening law can be used, the Nadai and Swift laws being well known examples.

By doing some standard uniaxial tests the hardening parameters can be determined. Performing the tests under different angles with respect to the rolling direction (RD), e.g. 0°, 45°, and 90°, and measuring the contraction in transverse direction (TD) enables one to calculate the stress–strain curves and the anisotropy factors. Together with an appropriate yield criterion, this is enough information to define the hardening behavior in most commercial FE software.

2.2.2. Strain path dependency

In most sheet metal forming processes the strain rate and strain path are not constant. The influence of strain rate can be predicted with strain rate dependent hardening laws [17,18]. Strain path dependency is an upcoming item to improve the predictions with FE-simulations. The current hardening models can be divided in three groups; isotropic hardening; kinematic hardening and strain path dependent models.

Isotropic hardening describes the evolution of the "growth" of the yield surface and is able to accurately reproduce the results of uniaxial tests. Kinematic hardening describes the movement of the yield surface in the principal stress space. Reverse loading, and more specifically the Bauschinger effect, can be modeled with this method. The modeling of the saturation of the yield stress after a stress reversal is improved with these models. Some more advanced modeling is done by [19].

The third group contains models that can describe arbitrary strain path changes. This is quite complex, because it requires information about the history of the strain path. Schmitt et al. [20] made a first step by introducing a measure for the strain path change:

$$\theta = \frac{\dot{\boldsymbol{\varepsilon}}_1^{\mathrm{p}} : \dot{\boldsymbol{\varepsilon}}_2^{\mathrm{p}}}{\|\dot{\boldsymbol{\varepsilon}}_1^{\mathrm{p}}\| \cdot \|\dot{\boldsymbol{\varepsilon}}_2^{\mathrm{p}}\|}, \tag{1}$$

where the subscripts 1 and 2 represent the situation before and after the strain path change, respectively. For a monotonic strain path, θ equals 1, for a reverse test θ equals -1 and θ equals 0 corresponds to an orthogonal test. Indeed, any value between -1 and 1 is possible, but these three situations are the extremes. Commonly, strain path dependent models are constructed in such a way that the behavior of an arbitrary strain path change θ is interpolated between the behavior of two reference tests. Viatkina et al. [21,22] have developed a model specifically for FCC-material (e.g. aluminum). Teodosiu and Hu [23] have developed a semi-physical material model that operates on macro-scale and is probably the most well-known model, see also [24,25]. It uses 13 material parameters that have to be determined from uniaxial, reverse and orthogonal tests. It is only compatible with the Hill'48 yield surface. The flexibility is good, but the number of tests is quite large. The model describes the strength of the material by means of the fourth order tensor $\boldsymbol{S}$ in the current strain direction $\boldsymbol{S}_{\mathrm{D}}$ and in the latent, or complementary, direction $\boldsymbol{S}_{\mathrm{L}}$:

$$\mathbf{S} = \mathbf{S}_{\mathrm{D}} + \mathbf{S}_{\mathrm{L}}. \tag{2}$$

During every increment in the calculation the strength is evaluated, but also the division between the directional and latent part is determined, which depend on the strain path change. This is then further evaluated in terms of isotropic and kinematic hardening. This material model is able to describe all observed strain path effects in literature: the Bauschinger effect and the plateau in stress after a stress reversal in a reverse test, the overshoot in stress and work softening after an orthogonal test. Parallel to the macro-model, also a micro-model has been developed [26,27]. In general, the computational effort and the large number of tests that have to be done to obtain a reliable material model are the major drawbacks of these methods.

2.2.3. Phase transformations

In Section 2.1.3, it is introduced that the rate of martensitic transformation is influenced by the mechanical driving force and the amount of nucleation sites for martensitic plates. In this section these concepts will be further discussed. A typical strain induced transformation curve is shown in Fig. 3.

For transformation to occur it is known that an energy barrier has to be overcome. This energy barrier is dictated mainly by temperature and can be calculated employing thermodynamics equations. The relative free energies of austenite and martensite are calculated with respect to temperature and the difference of these two determines how much more energy must be supplied to the material to have a spontaneous phase transformation. It is found in literature that this relation is linear and the barrier decreases with increasing temperature [13] as shown in Fig. 4.

Fig. 4 shows the amount of driving force $\Delta G^{\mathrm{critical}}$, necessary for martensite transformation at temperature M_S (martensite start temperature). At M_S this critical

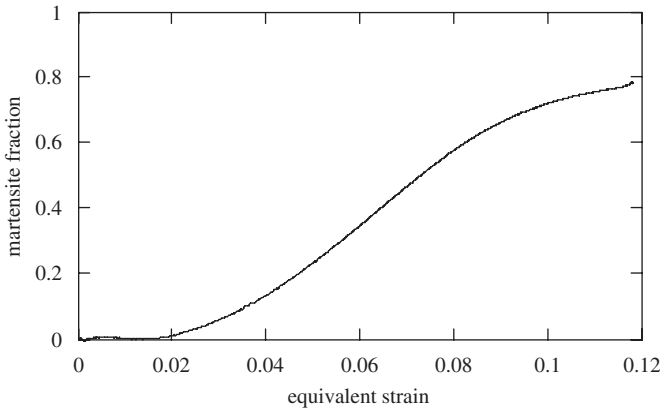

Fig. 3. Martensite fraction vs equivalent strain curve of ASTM-A 564 during a tensile test.

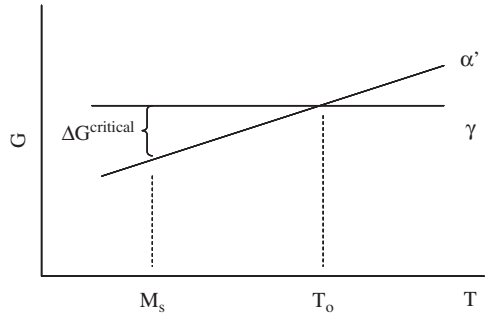

Fig. 4. The free energy curves of austenite γ and martensite α'. The difference between the two curves dictates the chemical driving force.

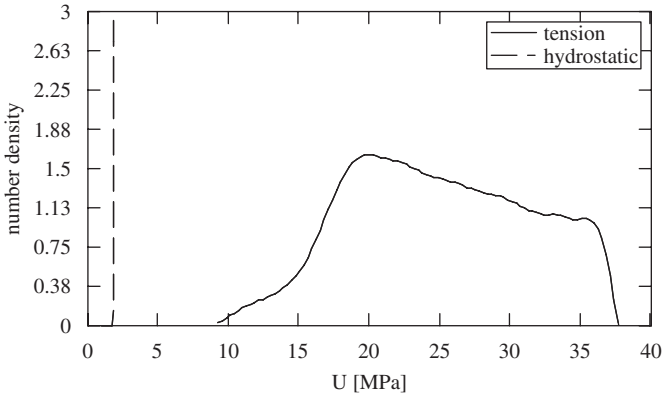

Fig. 5. Distribution of resolved maximum driving force throughout the material.

driving force equals the chemically stored driving force (difference between the two curves). However, for higher temperatures, the chemically stored driving force is not sufficient to let austenite transform to martensite. The difference in driving force (i.e. $\Delta G^{\text{critical}}$ minus ΔG at temperature T) must then be supplied by a mechanical driving force.

One of the most challenging issues is to calculate the mechanical driving force needed for the transformation. Driving force is the opposite of the amount of work U that would be done by transformation under the applied stress, i.e. for small strains, the work is calculated as the amount of strain multiplied by the amount of stress [13]. Consequently, one has to know how much strain the transformation would cause in order to know the driving force. Fortunately, it is possible to calculate the transformation strain using the lattice correspondence of austenite and martensite [28]. Due to the high symmetry of the austenite lattice however, in a single crystal there exists multiple possible strains (variants) of which only the favorable ones can transform. There are micromechanical models which consider all the variants and track their growth separately [29,30].

However, micromechanical models cannot be used to simulate the overall material behavior because it is computationally too expensive. Therefore, some of the microscale parameters are averaged over many grains, yielding a mesoscale model which is presented in the remainder of this section. Knowing the current state of the available driving force it is already possible to comment on the possibility of transformation. If the energy barrier is breached by some grains then transformation would start. This is sufficient for prediction of the change of the M_S (martensite start temperature) when quenched under mechanical loading. Since M_S is defined as the temperature at which the first trace of martensite plates appear, it is possible to calculate the temperature where the maximum resolved driving force in any grain exceeds the critical driving force. In Fig. 5 the calculated distribution of maximum resolved driving force in grains throughout the material is plotted. It is assumed that the same stress on the material point acts on each grain. The figure shows that under hydrostatic stress all the variants gain the same amount of mechanical driving force whereas under tension, due to the shear component of loading, there is a distribution of the driving force among grains. While Fig. 4 shows the critical driving force ($\Delta G^{\text{critical}}$) and the current *chemical* driving force at temperature T, Fig. 5 shows the distribution of the *mechanical* driving force stored in the material grains. If the required amount of additional energy is known, then Fig. 5 shows what fraction of the grains have that energy, hence giving a clue on how the transformation would proceed. Additionally, this figure clearly shows that the formation of martensite strongly depends on the loading situation.

However, to have the complete picture of strain induced transformation, it is necessary to take the nucleation phenomenon into account. Using the formulation supplied by Olson and Cohen [16], it is possible to approximate the formation of nucleation sites in the form of shear-band intersections with respect to equivalent plastic strain. Their formulation utilizes the averaging of microscale phenomena via a phenomenological relation and can be integrated in a macroscale constitutive model.

Another important issue is the homogenization of the microstructure for plastic strain and stress. Since the relative hardness levels of austenite and martensite are significantly different, plastic strain will tend to accumulate in austenite while the stresses build up in martensite. During the update of stress therefore the total strain must be decomposed into elastic, plastic and transformation parts as $\varepsilon = \varepsilon^{\text{e}} + \varepsilon^{\text{p}} + \varepsilon^{\text{tr}}$ and then the plastic strain must be distributed into phases. Using this stress and strain information the amount of transformation can be iteratively solved as in the model by Stringfellow et al. [31].

To conclude, the simulation of the mechanical behavior of metastable steels requires physically valid material models for describing the strain-induced martensitic transformations. Therefore, the validity of the constitutive model strongly depends on the model that describes the phenomenon of austenite to martensite transition which takes place in microscale. There are atomistic descriptions of this transition in literature which enable the calculation of certain parameters such as the mechanical driving force

and the number of nucleation sites. Micromechanical models consider a length scale of several grains and thus can employ these relations directly to simulate the transformation. However, due to computational reasons it is not possible to simulate the overall behavior of the material with these models. In order to get to macroscale efficiently, some of the parameters must be averaged over many grains with random or textured orientations. Doing this, a portion of the scientific accuracy is sacrificed to gain industrial applicability. The advantage of macroscale models is the availability to use mechanical tests to determine unknown parameters introduced by phenomenological relations which, on the contrary, is a very challenging task for micromechanical models.

2.3. Material testing

A new biaxial testing device for sheet material is developed at the University of Twente [32]. The equipment, Fig. 6, can deform a sample in shear and tensile directions. The actuators for the shear and tensile directions are controlled individually making all arbitrarily combinations of shear and tensile deformation possible. The width/height ratio of the deformation zone is chosen quite large to obtain a homogeneous shear deformation in the material. Due to this high ratio, a plane strain condition is introduced in horizontal direction when applying tensile deformation. The covered domain is depicted on the right-hand side of Fig. 7.

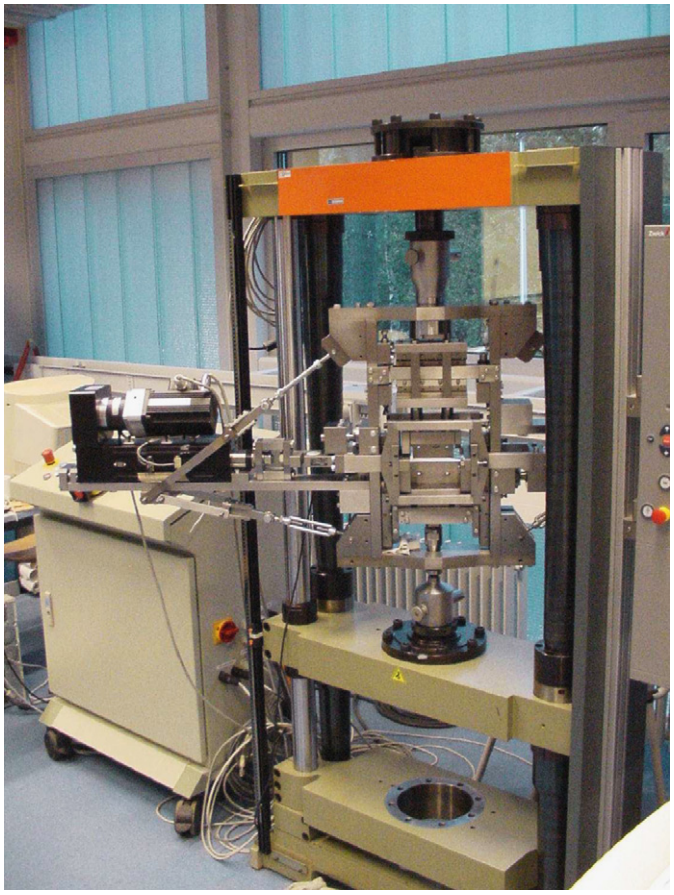

Fig. 6. The test equipment.

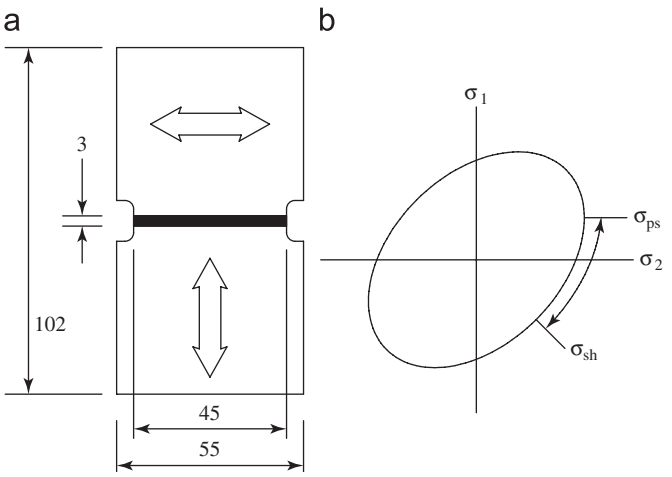

Fig. 7. (a) Sample with the dimension in mm, the black zone represents the deformation zone and the arrows represent the deformation direction. (b) The principal stress space with the covered domain.

Dots of silicone cement are attached to the surface of the deformation zone of the sample; these are tracked by a camera and the co-ordinates of the dots are used to determine the strains in the plane of the sample. The stresses in tensile and shear directions are easily determined by measuring the forces in these directions and by using the geometry of the sample. The stress in horizontal direction is more complicated because of the plane strain boundary condition. As a result the position of the stress state in the principal stress space is unknown due to the missing stress component [33].

The machine is capable of doing numerous experiments, but with the extra possibilities also some extra complexity is introduced. A good example that illustrates this point is a test with a prescribed strain path. For this, it is important to know that the displacement of the clamps is prescribed, and is not adjusted during the test. Due to the strain path it is possible that stress relaxation takes place. However, due to its stiffness, the test frame gives an extra deformation to the sample and hereby disrupting the intended strain path [34]. Compensation for this kind of problems have to be made to get the prescribed strain paths. An advantage of this testing machine over a cruciform biaxial tester is the homogeneity of the deformation [35,36]. The deformation zone in such a sample is hard to deform homogeneously and therefore these tests are mostly used for small strains in the plastic zone [35]. However, the elasto-plastic transition for various combinations of strains is still interesting for the determination of a yield locus [36].

2.3.1. Reverse tests

In this section some results of reverse tests in simple shear are discussed. Two materials are tested: DC06 steel and AA5182 aluminum. Both metals are used in the automotive industry. The results are depicted in Fig. 8.

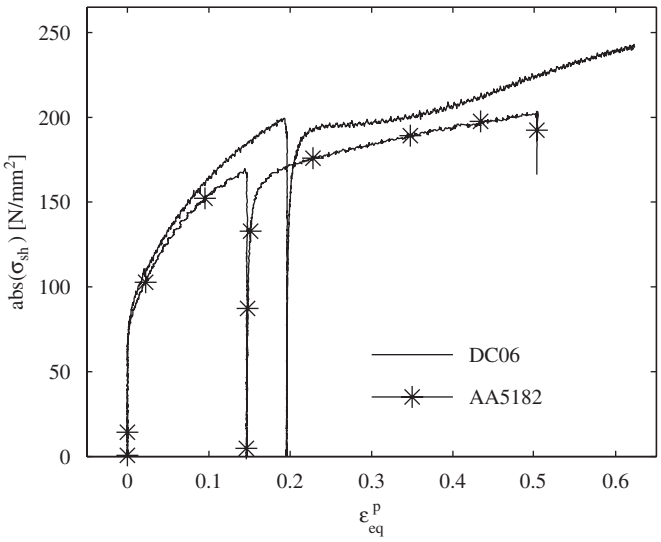

Fig. 8. The absolute shear stress versus the equivalent plastic strain for DC06 and AA5182 in a reverse loading experiment.

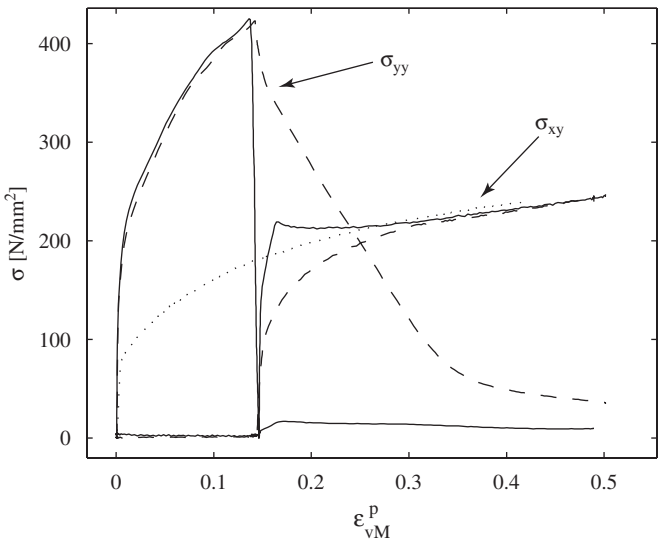

Fig. 9. Measurements on the tests with a sudden and a gradual strain path, indicated by solid and dashed lines, respectively. The dotted line indicates the monotonic simple shear test.

The amount of shear deformation in the two tests differ slightly, primarily due to slip in the clamps of the sample. Also, the elasticity of the test frame hampers the maximum achieved strain. During the first stroke, the dislocation sheets are developed and during this process dislocations migrate to these barriers. Once stuck there they hamper further deformation because they reject dislocations of the same sign. If the deformation direction is reversed, these dislocations migrate in opposite direction and enter "open space" where they can migrate without any trouble to the barrier at opposite side. Here the process repeats itself and the pile up develops again whereby the increase in stress converges to a saturation rate. This is illustrated by a hardening rate that hardly differs from the elastic behavior in the reverse stroke.

The BCC material (e.g. steel) clearly shows a plateau in stress after the reversal, after that the material resumes hardening. The aluminum however does not show this plateau, but resumes hardening with almost the same rate as in the first stroke. Both materials exhibit the Bauschinger effect, although the DC06 has a distinct difference in yield stress compared to the aluminum. It is mentioned that there is a distinction in evolution of the Bauschinger effect. Although not depicted, more strain in the first stroke gives more Bauschinger effect for the DC06, while the AA5182 does not show any increase.

2.3.2. Orthogonal tests

The orthogonal tests shown here are performed on the DC06 steel that has been used in the reverse tests as well. The sample is first loaded in tensile direction after which the material is loaded in shear direction. In one case the strain path change is suddenly introduced while in the other case the tensile deformation and shear deformation have a bit of overlap leading to a gradual strain path change.

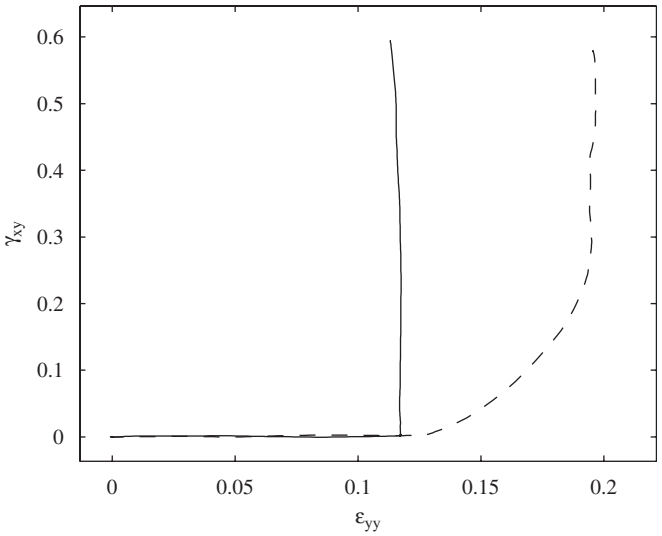

Fig. 10. Measurements on the tests with a sudden and a gradual strain path, indicated by solid and dashed lines, respectively.

In Fig. 9 the measured stresses are indicated. It shows that the different strain paths have quite different resulting stress paths. The test where the strain path change is introduced gradually shows a shear stress that gradually converges to the simple shear test. This is in contradiction to the test where the strain path change is introduced suddenly. The shear stress increases rapidly and shows an overshoot before dropping back to the level of the simple shear test. The stress in tensile direction shows the same features. The test with a sudden strain path change shows a rapid decrease in stress, while the test with a gradual strain path change shows a gradual decrease of stress. During the tests, the stress state moves from the plane strain point to the shear point.

It is assumed that a sudden strain path change, see Fig. 10, hampers the initial deformation and hence requires a large stress. The dislocations that tend to move in the orthogonal direction are restricted in their movement by the dislocation sheets. At a certain stress level the force becomes too high and microbands occur; these are channels of relatively dislocation-free areas that penetrate the dislocation sheets. Once these have been formed dislocations can migrate more easily through the material and hence require less stress, explaining the softening after the overshoot. The abovementioned results show that for an accurate modeling of material behavior, strain path dependency has to be accounted for.

2.3.3. Phase transformation tests

In order to verify and quantify the phenomena described in Sections 2.1.3 and 2.2.3 some mechanical tests are necessary. As discussed earlier there are tests which lead to conclusions such as the small particle tests by Magee [14], which proves that martensite nucleates heterogeneously and furthermore there is a potential distribution of defects. Additionally, it is known theoretically that the hydrostatic stress has a very significant effect on the rate of transformation deduced from the fact that transformation produces a volumetric expansion, and with hydrostatic stress, this makes a positive work [13]. Also, since expansion is isotropic and of the same amount for all the martensitic variants, this work is constant, which leads to the conclusion that the effect of hydrostatic stress is a linear increase in the mechanical driving force. There are multi-axial experiments carried out to quantify this phenomenon as in [11,37,38].

There are however not many experiments that directly relate the nucleation of martensite to plastic strain, except for Olson et al. [16] which is based on the role of shear band intersections on nucleation. In the nucleation theory of martensite the importance of initial nucleation sites and the autocatalytic effect is emphasized. To verify that this phenomenon is applicable to strain induced transformation, additional tests are necessary.

Considering the need for mechanical tests in the above-mentioned topics, some tests have been carried out with the biaxial tester described in the introduction of Section 2.3. With this equipment it is possible to attain deformation paths that can stimulate different stress states within the material. Hence, the visualization of the effect of stress state on the rate of transformation is achieved to the extent of the capabilities of the setup. To monitor the transformation a magnetic sensor is used. The sensor exploits the fact that martensite is ferromagnetic whereas austenite is paramagnetic meaning there is a significant difference between their magnetic permeability values. A series of tests have been carried out with proportional deformation paths to quantify the effect of hydrostatic stress on the rate and the results are plotted in Fig. 11. The material ASTM-A 564 is completely austenitic at room temperature and can transform 100% with the aid of mechanical deformation.

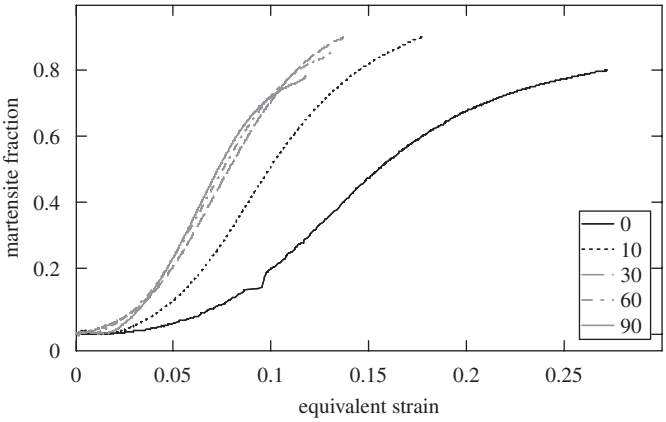

Fig. 11. Martensite fraction vs equivalent strain curve of ASTM-A 564 during proportional tests. Legend denotes the arctangent of rate of tension over rate of shear.

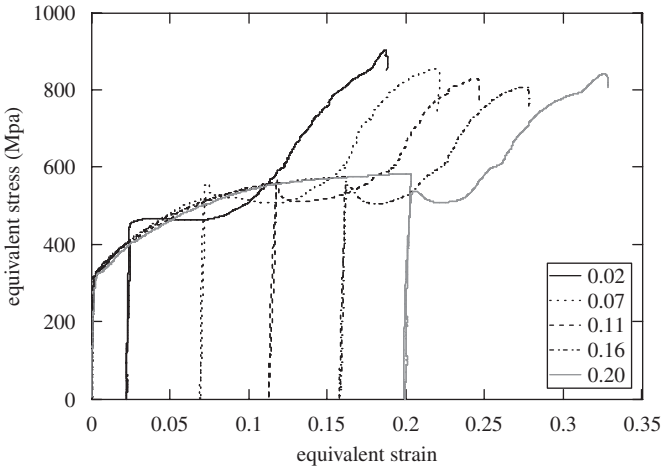

Fig. 12. Stress vs strain curves of ASTM-A 564 during tensile tests including prestraining at high temperature.

The exact amount of hydrostatic stress is not attainable with this setup. However, it is clear from the figure that it significantly affects the rate. A point to mention here is that all the curves have the same shape which proves that the effect of hydrostatic stress is isotropic and homogeneous. These experiments have also lead to quantitative results that show that the effect is linear.

To observe the effect of plastic strain alone is a challenging task since transformation is affected by many variables. However, utilizing some theoretical knowledge on the transformation it is possible to eliminate some of these variables. It is known that the chemical driving force is a function of temperature and decreases with increasing temperature and that transformation starts only when the total driving force exceeds a limit. Thus, if the material is strained at a high temperature, then transformation will be retarded while still being plastically strained. After this treatment it is possible to observe the effect of plastic strain on the rate of transformation. Fig. 12 shows the result of one of these experiments.

It is clear from the figure that there is a very pronounced effect of prestraining on the rate of transformation. These results prove some of the theories in the literature such as the creation of nucleation sites with plastic strain and the consumption of the ones with potencies high enough to be activated by the applied stress during the deformation at room temperature. Therefore, in the constitutive modeling of these types of steels it is possible to build algorithms in multiscale which can make use of the phenomena in micro- and mesoscales and transfer the averaged results to macroscale.

3. Failure

Damage, the degradation of material properties, and fracture are important criteria in the design of products and processes. In most cases cracks must be avoided in order to fulfill the product specifications. However, some products and processes rely on the controlled growth of damage and/or cracks in order to obtain a certain functionality or shape, e.g. sheet metal cutting.

Most metals at room temperature show a ductile failure mechanism, which consists of three stages—the nucleation, growth and coalescence of voids. Voids nucleate at inclusions or precipitates and grow under the applied loads. A microcrack is formed when the matrix between the voids fails. Finally these microcracks propagate by coalescence with voids in front of the crack tip. The spacing and distribution of void nucleating inclusions is the key microstructural feature for setting the crack growth resistance. For structural metals, the size of the void nucleating particles ranges from 0.1 to 100 μm, with volume fractions of a few percent [39–41].

In case of multi-step forming processes, damage induced in previous forming steps may influence the response in subsequent steps. Furthermore, the development of damage during forming may be important for the properties of the final product. For example the crash behavior of a formed product may deteriorate due to the presence of damage. The design of processes and products can benefit from an integral management of the amount of damage introduced, by avoiding damage in critical locations in the product, by tolerating a certain amount of damage in non-critical locations or even by applying damage on purpose to control the crack trajectories. Therefore accurate predictions of the damage are required.

A conventional method to predict failure is the use of FLCs, Section 3.1. However, the applicability of FLC's is limited. Ductile damage models, as described in Section 3.2, can be used instead of or complementary to the FLC approach to improve the prediction of failure. The performance of these damage models is shown in Section 3.3.

3.1. Forming limit curve

Traditional assessments of the formability of sheet metal materials are based on the appearance of geometrical instabilities, e.g. necking of the sheet. Necking occurs when the strain hardening exhibited by the material can no longer compensate the thickness reduction which results from large in-plane strains. As a consequence, the plastic deformation becomes unstable and localizes in a narrow region, resulting in a crack. A commonly used method to predict geometrical instabilities in sheet metal forming processes is the FLC. Necking will occur when the strains in the product exceed the FLC in the (in-plane) principal strain space. In such cases the process has to be adapted.

However, the use of an FLC has some limitations:

- The FLC has been measured or calculated with the assumption that the strain state is constant over the thickness of the sheet. In sheet bending processes with small radius-to-thickness (R/t) ratios, the outer layer of the sheet is unstable, but the sheet as a whole is not. Therefore the formation of a neck is impossible. An example is the hemming process;
- Non-traditional forming materials with less formability, such as aluminum, titanium and high-strength steels, often fail due to physical instabilities, even before necking starts. Even in situations where physical degradation is not the main failure mechanism, it may have a significant effect on and interact with the geometrical necking mechanism [42].
- An FLC is only valid for proportional strain paths. However, most forming processes involve highly non-proportional strain paths, for instance due to multiple forming steps, see Section 2.2.2.
- Many forming processes take place at elevated temperatures, at high (strain) rates and are accompanied by complex microstructural changes such as phase changes, see Section 2.2.3. These mutually strongly coupled phenomena, which also interact with the development of damage, cannot easily be described in terms of an FLC.

3.2. Damage models

3.2.1. Fracture criteria

Indicators which calculate the probability of fracture as a function of the deformation and stress history are gradually becoming available in simulation software. These indicators are mostly used for bulk forming processes [43], but they can also be applied to sheet metal forming [44].

A simple indicator is the equivalent plastic strain. In practice, however, this criterion turns out to be a relatively poor predictor of damage. More accurate criteria include information on the stress state and history. Especially the stress triaxiality (hydrostatic stress divided by the equivalent stress) proves to be an important factor. A superimposed hydrostatic stress significantly increases the strain to fracture. Although some successes have been reported [43,44], the results are only valid for specific processes and materials. Therefore obtained results cannot be easily applied to new cases.

3.2.2. Local damage models

Contrary to the fracture criteria, local damage models aim to describe the interaction of damage growth and plastic flow. Examples of these damage models are the so-called Gurson Tvergaard Needleman family of models or Continuum Damage Models [45–47]. The damage is now incorporated into the constitutive relations, which leads to a redistribution of the stress and strain fields when the damage develops. Here, a scalar variable $\omega_p \in [0,1]$ is used to describe the degradation of the material properties (Eq. (3)).The material fails if the damage z exceeds the critical value z_c. Expressions for the damage values can be found in [45,46]. The overall stress can be written as the stress in the undamaged material σ_M multiplied by the factor $(1-\omega_p)$, the amount of undamaged material able to carry any load (Eq. (4)). The damage is included in the elastic properties and also in the yield function (Eq. (5)) in which the strain hardening competes with the damage softening.

$$\omega_p = \frac{z}{z_c}, \tag{3}$$

$$\sigma = (1-\omega_p)\sigma_M, \tag{4}$$

$$\sigma_y = (1-\omega_p) f(\varepsilon^p, ..). \tag{5}$$

Crack growth can be seen as the natural outcome of the degradation process in these models. However, it is well-known that these models suffer from a pathological dependence of the element size and direction. The localization will likely occur in only one row of elements.

3.2.3. Non-local damage models

Non-local models have been introduced to overcome the mesh dependency of standard softening continua [48]. In this article, a non-local damage model will be presented, as described comprehensively by Mediavilla [49] and Engelen [50].

A non-local damage variable $\bar{z}$ is introduced which is calculated from the local damage z using a Helmholtz partial differential equation. This model contains a length scale. The degradation ω_p is a function of the non-local damage $\bar{z}$.

$$\omega_p = \frac{\bar{z}}{\bar{z}_c}. \tag{6}$$

In non-local damage models, the length scale is used to average the localization over more than one element; the width of the localization depends on the length scale and not on the element size.

3.3. Three-point bending example

The damage models described in the previous section will be demonstrated in this section with simulations of a three point bending test (Fig. 13).

The shown damage models contain some extra material parameters, which have to be determined experimentally [51,52]. At the moment no established identification method exists.

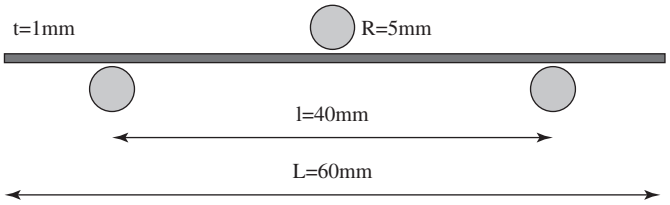

Fig. 13. Three point bending test.

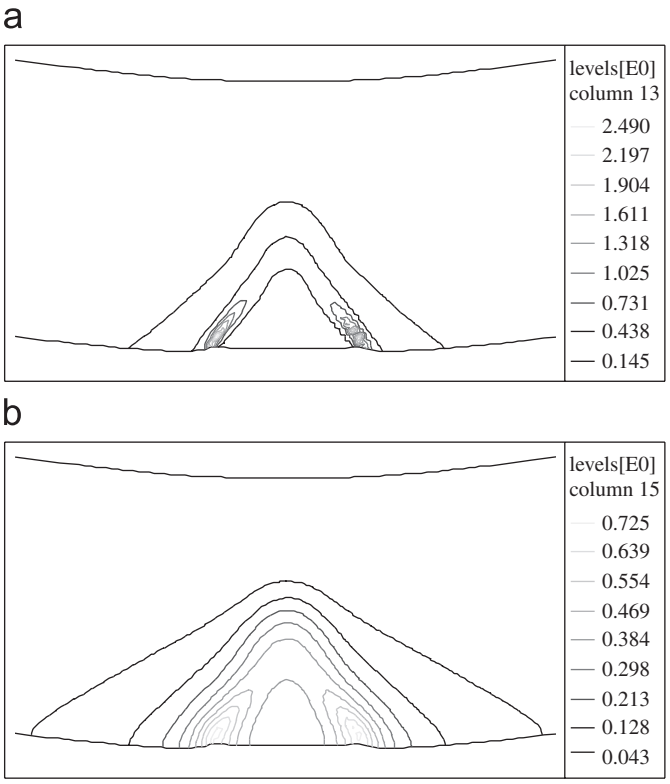

Fig. 14. Non-local values (length scale = 0.05) calculated from the local values (mesh 2). (a) local value and (b) non-local value.

An elasto-plastic material model is used with Young's modulus of 210 GPa and Poisson ratio of 0.3 and the Nadai hardening law. The used damage model accounts for the influence of the hydrostatic stress [51]. Therefore damage will start growing at the outer radius of the bend sheet. The critical values of the damage z_c and $\bar{z}_c$ are taken to be equal to 0.5, which already results in failure for very small bending angles.

Three different meshes—mesh1, mesh2 and mesh3—have been used for the simulations, which have decreasing mesh sizes of 0.04/0.02/0.01 mm respectively, in the horizontal direction. The mesh size in vertical direction is 0.05 mm and constant.

Fig. 14 shows the difference between the local and the non-local model. It can be seen that the non-local model spreads the damage in the localization band over a larger area.

Different failure patterns can be obtained by changing the value of the length scale as shown in the Figs. 15 and 16. Small shear-bands can be seen for the local model (i.e. $l = 0.0$). These bands get wider for increasing length scale. For large length scales ($l = 0.2$) these bands disappear completely.

Similar shear-bands are presented in investigations on the bendability of aluminum [53,54]. The difference in microstructure between the alloys should be captured in the non-local model by a different length scale and damage evolution law.

In Fig. 17(a) the force–displacement diagram is shown for different length scales. The larger the length scale, the more ductile is the response. Fig. 17(b) shows the mesh dependency of the local damage model, whereas the results of the non-local model are almost insensitive to the mesh size, Fig. 17(c).

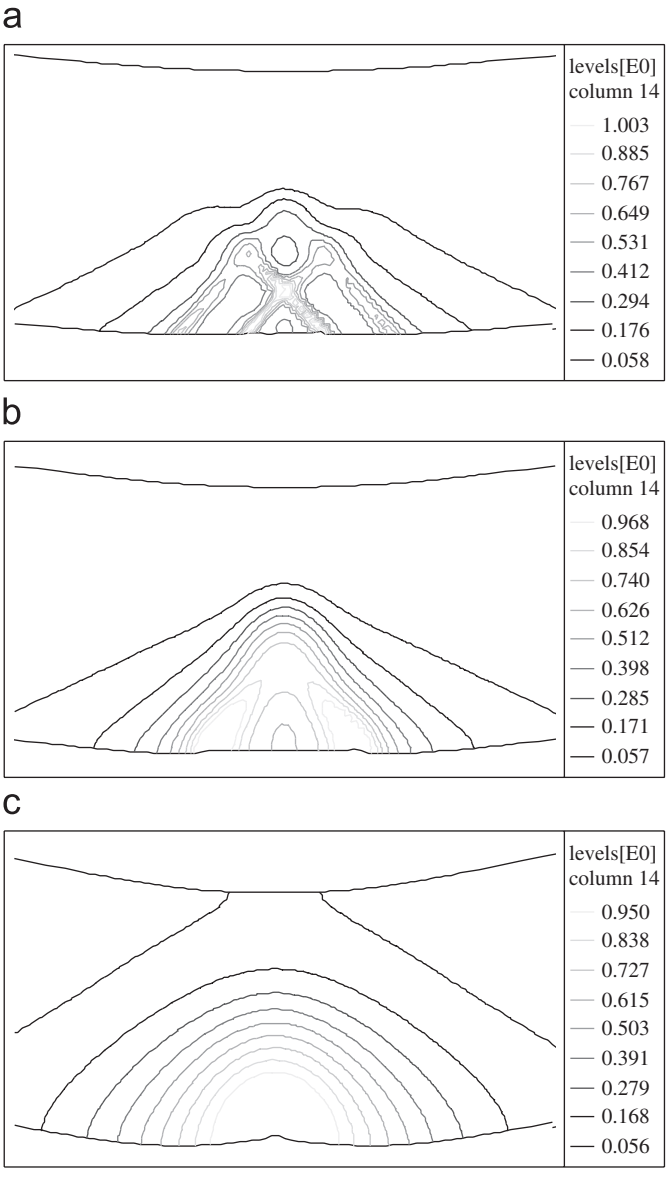

Fig. 15. Degradation ω_p (mesh 2). (a) local, (b) l = 0.05 and (c) l = 0.2.

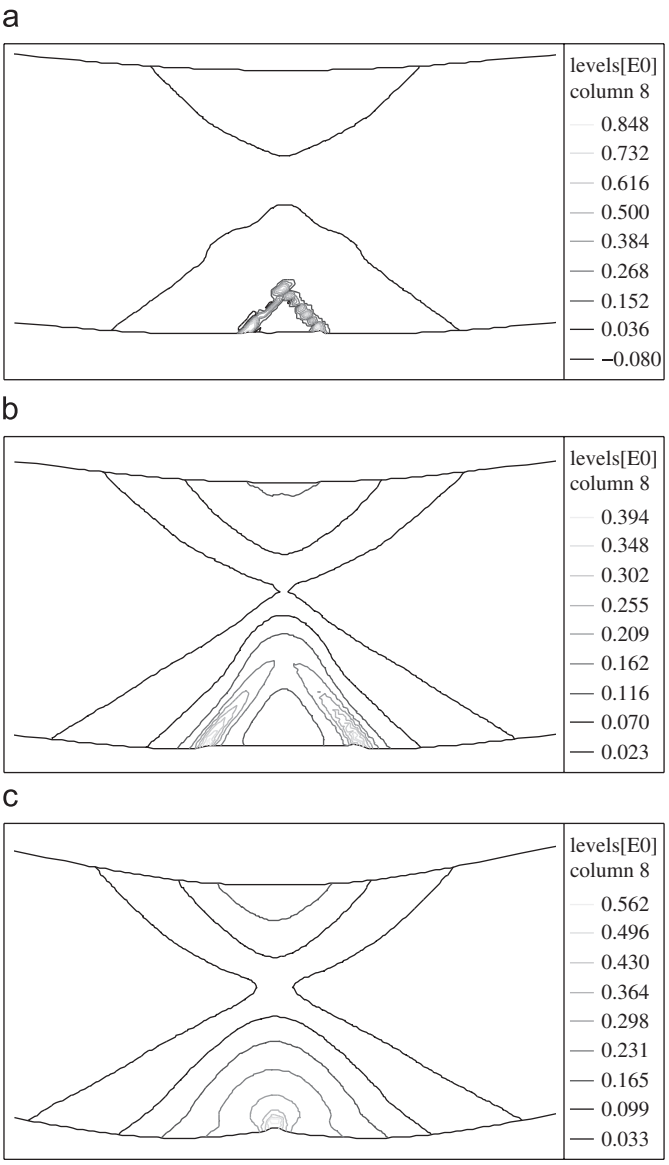

Fig. 16. Equivalent plastic strain (mesh 2). (a) local, (b) l = 0.05 and (c) l = 0.2.

4. Discussion and future trends

In the beginning of material modeling, simple models were used to describe the hardening behavior and yielding conditions. These models proved to be sufficient for a small range of materials with a straightforward behavior. However, in the last decades the industrial requirements for an accurate simulation increased together with the use of new advanced materials. These advanced materials show complex material behavior such as strain rate sensitivity, strain path dependency, non-isotropic hardening, phase transformations etc. To come up with material models which can describe these effects, a thorough knowledge of the physics behind this behavior is required. Studying these physics can be done on multiscale level, from microscale to macroscale. The advantage of microscale models is that they are able to directly simulate complex effects,

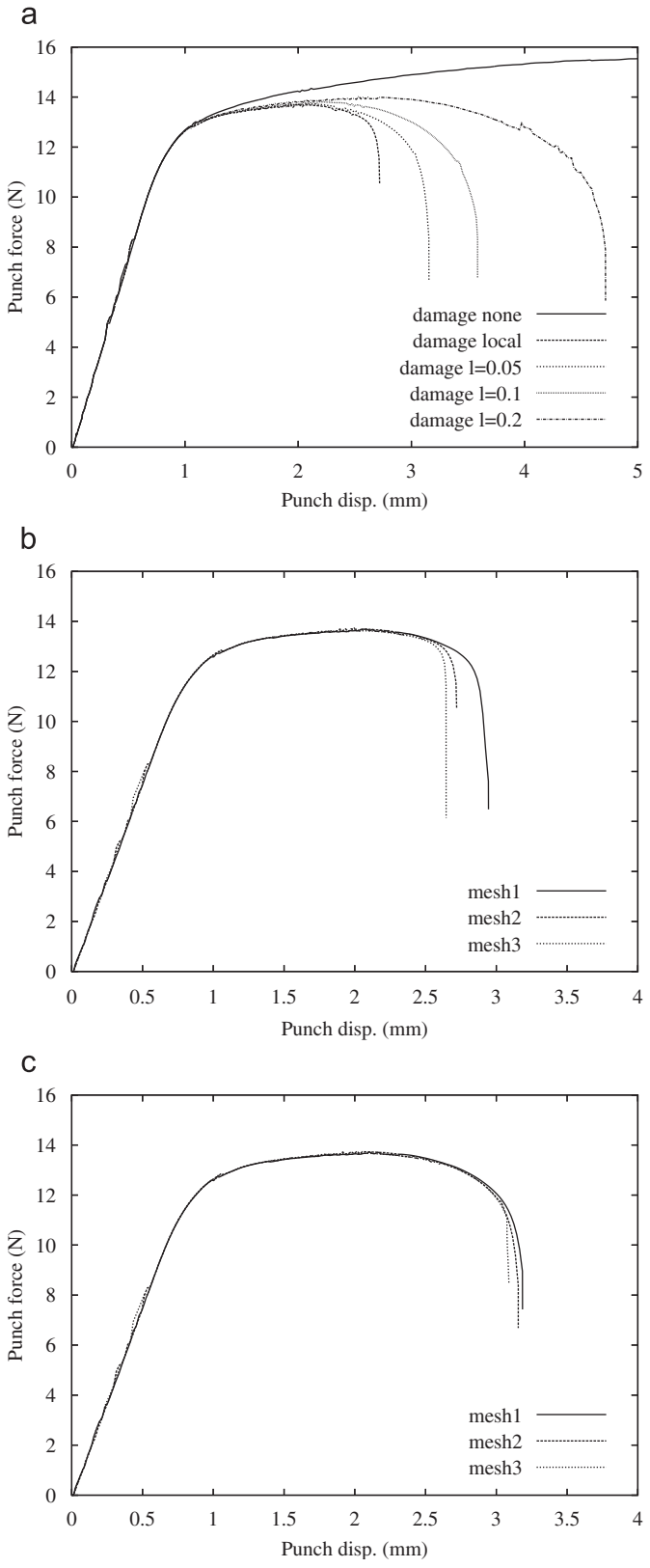

Fig. 17. Force displacement curves for different meshes and length scales. (a) mesh 2, (b) local damage model and (c) non-local model $l = 0.05$.

e.g. martensitic transformation, however at high computational costs. Hence, the overall material behavior cannot be captured by these models; so, macromechanical material models must be used for this purpose. A macroscopic material model estimates the micromechanical material behavior without actually performing calculations on grain size level. In this way industrial applicability is gained by sacrificing some of the accuracy. Hence, today's challenge is to develop macroscopic models which meet tomorrow's industrial requirements on both accuracy and applicability.

The prediction of failure is improved by using damage models. Non-local damage models are favored to the local damage models, since they do not show mesh size dependency. It is shown that the use of non-local damage models will improve the understanding of the failure mechanisms. Using these models complementary to the FLC approach can result in better failure predictions for critical applications. However, there are some drawbacks in using the non-local damage models. The length scale in the non-local model determines the element size in the damaged areas as it should be larger than the element size in order to capture the gradients properly. Ideally this length scale is related to the microstructure. However, especially in 3D simulation, small length scales lead to a large number of elements. In practice the length scale might be chosen larger in order to decrease the problem size. Also adaptive remeshing of the damaged area might solve this problem [49]. The application of the non-local method to shell elements is not straightforward as element sizes are normally larger than the thickness and length scales smaller than the thickness. Furthermore, details smaller than the thickness, like the shear-bands in the bending problem, cannot be captured using the Kirchhoff/Love or Mindlin plate bending assumptions.

Besides, crack propagation is not taken into account in this article. It is often modeled by element erosion, i.e. elements in which the damage criterion has been reached are removed from the problem and the simulation is continued on this updated geometry. Element erosion results in mass loss and a faceted crack surface. This may have a strong influence on the local stress and strain distributions and may lead to numerical instabilities. Alternative computational techniques to describe evolving cracks, such as remeshing or partition-of-unity methods, are not sufficiently well developed and therefore not yet used very often for industrial cases.

Acknowledgements

Most of the research has been carried out under projects in the framework of the Netherlands Institute for Metals Research (NIMR) and the FOM-NIMR research programme. The industrial partners co-operating in this project are gratefully acknowledged for their useful contributions to this research.

References

[1] O. Cazacu, B. Plunkett, F. Barlat, Orthotropic yield criterion for hexagonal closed packed metals, International Journal of Plasticity 22 (2006) 1171–1194.

[2] J. Yoon, F. Barlat, R. Dick, M. Karabin, Prediction of six or eight ears in a drawn cup based on a new anisotropic yield function, International Journal of Plasticity 22 (2006) 174–193.
[3] H. Vegter, A. Van den Boogaard, A plane stress yield function for anisotropic material by interpolation of biaxial stress states, International Journal of Plasticity 22 (2006) 557–580.
[4] D. Banabic, T. Kuwabara, T. Balan, D. Comsa, An anisotropic yield criterion for sheet metals, Journal of Materials Processing Technology 157&158 (2004) 462–465.
[5] J.W. Steeds, Dislocation arrangement in copper single crystals as a function of strain, Proceedings of the Royal Society 292 (1966) 343–372.
[6] S. Thuillier, E. Rauch, Development of microbands in mild steel during cross loading, Acta Metallurgica et Materialia 42 (6) (1994) 1973–1983.
[7] S. Thuillier, E. Rauch, Interaction of microbands with grain boundaries in mild steel, Scripta Metallurgica et Materialia 32 (4) (1995) 541–546.
[8] E. Rauch, The stresses and work hardening rates of mild steel with different dislocation patterns, Materials Science and Engineering A 234–236 (1997) 653–656.
[9] G.E. Dieter, Mechanical Metallurgy, third ed., McGraw-Hill Book Company, 1987.
[10] J.G. Sevillano, P. van Houtte, E. Aernoudt, Large strains work hardening and textures, Progress in Materials Science 25 (1981) 69–412.
[11] J. Post, On the constitutive behavior of sandvik nanoflex, Ph.D. Thesis, University of Twente, 2004.
[12] G. Olson, W. Owen, Martensite: a tribute to Morris Cohen, ASM International, Materials Park, OH, 1992.
[13] J.R. Patel, M. Cohen, Criterion for the action of applied stress in the martensitic transformation, Acta Metallurgica 1 (1953) 531–538.
[14] C. Magee, The kinetics of martensite formation in small particles, Metallurgical Transactions 2 (1971) 2419–2430.
[15] S. Pati, M. Cohen, Kinetics of isothermal martensitic transformations in an iron-nickel-manganese alloy, Acta Metallurgica 19 (1971) 1327–1332.
[16] G. Olson, M. Cohen, Kinetics of strain-induced martensitic nucleation, Metallurgical Transactions 6A (1975) 791–795.
[17] P. van Liempt, Workhardening and substructural geometry of metals, Journal of Materials Processing Technology 45 (1994) 459–464.
[18] M. Goerdeler, G. Gottstein, A microstructural work hardening model based on three internal state variables, Materials Science and Engineering A 309-110 (2001) 377–381.
[19] J.L. Chaboche, On some modifications of kinematic hardening to improve the description of ratchetting effects, International Journal of Plasticity 7 (1991) 661–678.
[20] J. Schmitt, E. Aenoudt, B. Baudelet, Yield loci for polycrystalline metals without texture, Materials Science and Engineering 75 (1985) 13–20.
[21] E. Viatkina, W. Brekelmans, M. Geers, Strain path dependency in metal plasticity, Journal de Physique IV 105 (2003) 355–362.
[22] E. Viatkina, Micromechanical modelling of strain path dependency in fcc metals, Ph.D. Thesis, Eindhoven University of Technology, 2005.
[23] C. Teodosiu, Z. Hu, Evolution of the intergranular microstructure at moderate and large strains: modelling and computational significance, in: S.-F. Shen, P.R. Dawson (Eds.), Proceedings of NUMIFORM, Balkema, Rotterdam, 1995, pp. 173–182.
[24] A. Uenishi, C. Teodosiu, Constitutive modelling of the high strain rate behaviour of interstitial-free steel, International Journal of Plasticity 20 (2004) 915–936.
[25] H. Haddadi, S. Bouvier, M. Banu, C. Maier, C. Teodosiu, Towards an accurate description of the anisotropic behaviour of sheet metals under large plastic deformations: modelling, numerical analysis and identification, International Journal of Plasticity 22 (2006) 2226–2271.
[26] B. Peeters, M. Seefeldt, C. Teodosiu, S.R. Kalidindi, P. van Houtte, E. Aernoudt, Work-hardening/softening of b.c.c polycrystals during changing strain paths: I. an integrated model based on substructure and texture evolution, and its prediction of the stress–strain behaviour of an IF steall during two-stage strain paths, Acta Materialia 49 (2001) 1607–1619.
[27] B. Peeters, B. Bacroix, C. Teodosiu, P. van Houtte, E. Aernoudt, Work-hardening/softening of b.c.c polycrystals during changing strain paths: II. TEM observations of dislocation sheets in an IF steel during two-stage strain paths and their representation in terms of dislocation densities, Acta Materialia 49 (2001) 1621–1632.
[28] M. Wechsler, D. Lieberman, T. Read, On the theory of formation of martensite, Transactions of the AIME 197 (1953) 1503–1515.
[29] F. Marketz, F. Fischer, A micromechanical study on the coupling effect between microplastic deformation and martensitic transformation, Computational Materials Science 3 (1994) 307–325.
[30] M. Cherkaoui, M. Berveiller, X. Lemoine, Couplings between plasticity and martensitic phase transformation: overall behavior of polycrystalline trip steels, International Journal of Plasticity 16 (2000) 1215–1241.
[31] R. Stringfellow, D. Parks, G. Olson, A constitutive model for transformation induced plasticity accompanying strain-induced martensitic transformations in metastable austenitic steels, Acta Metallurgica et Materialia 40 (1992) 1703–1716.
[32] H.H. Pijlman, Sheet material characterisation by multi-axial experiments, Ph.D. Thesis, University of Twente, 2001.
[33] A. van den Boogaard, M. van Riel, J. Huétink, Evaluation of stresses in a combined plane strain-simple shear test, in: D. Banabic (Ed.), Proceedings of ESAFORM, Akapit, Cluj-Napoca, Romania, 2005, pp. 383–386.
[34] M. van Riel, A. van den Boogaard, J. Huétink, Non-proportional tests in a biaxial test facility, in: N. Juster, A. Rosochowski (Eds.), Proceedings of ESAFORM, Akapit, Glasgow, UK, 2006, pp. 323–326.
[35] T. Kuwabara, M. Kuroda, V. Tvergaard, K. Nomura, Use of abrupt strain path change for determining subsequent yield surface: experimental study with metal sheets, Acta Materialia 48 (2000) 2071–2079.
[36] D. Banabic, J. Huétink, Determination of the yield locus by means of temperature measurement, in: N. Juster, A. Rosochowski (Eds.), Proceedings of ESAFORM, Akapit, Glasgow, UK, 2006, pp. 359–362.
[37] M. Coret, S. Calloch, A. Combescure, Experimental study of the phase transformation plasticity of 16mnd5 low carbon steel induced by proportional and nonproportional biaxial loading paths, European Journal of Mechanics A/Solids 23 (2004) 823–842.
[38] Q. Furnémont, F. Delannay, P. Jacques, Experimental investigation of the influence of the stress state on the mechanical stability of austenite in multiphase steels, Journal de Pyhsique IV 112 (2003) 421–424.
[39] B. Dodd, Y. Bai, Ductile Fracture and Ductility, Applications to Metalworking, Academic press, London, 1987.
[40] P.F. Thomason, A view on ductile-fracture modelling, Fatigue and Fracture of Engineering Materials and Structures 21 (1998) 1105–1122.
[41] A. Benzerga, J. Beson, J. Pineau, Anisotropic ductile fracture part I: experiments, Acta Materialia 52 (2004) 4623–4638.
[42] M. Brunet, S. Mquil, F. Morestin, Analytical and experimental studies of necking in sheet metal forming processes, Journal of Materials Processing Technology 80&81 (1998) 40–46.
[43] B. Gouveia, J. Rodriques, P. Martins, Ductile fracture in metalworking: experimental and theoretical research, Journal of Materials Processing Technology 101 (2000) 52–63.
[44] H. Takuda, K. Mori, N. Hatta, The application of some criteria for ductile fracture to the prediction of the forming limit of sheet metals, Journal of Materials Processing Technology 95 (1999) 116–121.
[45] V. Tvergaard, Material failure by void growth to coalescence, Advanced in Applied Mechanics 27 (1990) 83–151.
[46] J. Lemaitre, Coupled elasto-plasticity and damage constitutive equations, Computer Methods in Applied Mechanics and Engineering 51 (1985) 31–49.

[47] A. Mkaddem, R. Hambli, A. Potiron, Comparison between gurson and lemaitre damage model in wiping and bending processes, International Journal of Advanced Manufacturing Technology 23 (2004) 451–461.
[48] G. Pijaudier-Cabot, Z. Bazant, Nonlocal damage theory, Journal of Engineering Mechanics-ASCE 113 (1987) 1512–1533.
[49] J. Mediavilla, R. Peerlings, M. Geers, An integrated continuous-discontinuous approach towards damage engineering in sheet metal forming processes, Engineering Fracture Mechanics 73 (7) (2006) 895–916.
[50] R. Engelen, M. Geers, F. Baaijens, Nonlocal implicit gradient-enhanced elasto-plasticity for the modelling of softening behaviour, International Journal of Plasticity 19 (2003) 403–433.
[51] A. Goijaerts, L. Govaert, F. Baaijens, Evaluation of ductile fracture models for different metals in blanking, Journal of Materials Processing Technology 110 (2001) 312–323.
[52] A. Mkaddem, F. Gassara, R. Hambli, A new procedure using the microhardness technique for sheet material damage characterisation, Journal of Materials Processing Technology 178 (2006) 111–118.
[53] J. Sarkar, T. Kutty, K. Conlon, D.S. Wilkinson, J. Embury, D. Lloyd, Tensile and bending properties of AA5754 aluminium alloys, Materials Science and Engineering A 316 (2001) 205–209.
[54] W.B. Lievers, A.K. Pilkey, D.J. Lloyd, The influence of iron content on the bendability of AA6111 sheet, Materials Science and Engineering A 361 (1&2) (2003) 312–320.